Materialia 6 (2019) 100331

Contents lists available at ScienceDirect

Materialia

journal homepage: www.elsevier.com/locate/mtla

Full Length Article

Time-evolution of NIR absorption in hydroxide-catalysis bonds

Iain W. Martin[a,*], Jessica Steinlechner[a,b], Anna-Maria A. van Veggel[a], Zeno Tornasi[a], Angus S. Bell[a], Jim Hough[a], Sheila Rowan[a]

[a] SUPA, School of Physics and Astronomy, University of Glasgow, Glasgow G12 8QQ, Scotland, United Kingdom
[b] Institut für Laserphysik and Zentrum für Optische Quantentechnologien, Universität Hamburg, Luruper Chaussee 149, Hamburg 22761, Germany

ARTICLE INFO

MSC:
00-01
99-00

Keywords:
Optical absorption
Hydroxide catalysis bonding
Precision jointing techniques
Water absorption
Optically transmissive bonds
Water migration

ABSTRACT

Hydroxide-catalysis bonding is a powerful precision jointing technique. It is used to construct opto-mechanical systems, e.g. in gravitational-wave detectors or satellite-based telescopes, and for optical applications such as high-power laser-crystal assemblies or transmissive optical components. Here we present studies of the optical absorption of such a bond over a period of 38 days after bonding. We find significant absorption at 1550 nm and 2000 nm, while it is negligible at 1064 nm. We show a factor of four reduction in absorption over the observed period, which could increase the tolerable power in transmissive bonded optics. Based on the absorption ratio found at different wavelengths, we conclude that the absorption is most likely dominated by water migrating out of the bond by two mechanisms.

1. Introduction

Hydroxide-catalysis bonding is a precision jointing technique, which has been established for highly-specialized applications of opto-mechanical systems. It was first developed, patented and applied by Gwo [1–3] for the Gravity Probe B satellite mission [4] in which it was used to join the telescope's fused-silica components and optical bench together. The technique has also been used for the LISA pathfinder satellite mission, which was a very successful technology demonstrator for the planned space-based LISA gravitational-wave detector [5]. The mechanical properties of hydroxide-catalysis bonds are ideally suited for use in precision applications, such as bonding fused-silica parts together or silica to Zerodur and, as recently shown, for bonding of phosphate glasses [6]. Such bonds are suitable for applications in ultra-high vacuum and at cryogenic temperatures, as well as being extremely strong and stable [7].

Hydroxide-catalysis bonding has been further developed for the quasi-monolithic fused-silica test-mass suspensions of ground-based gravitational-wave detectors; first for GEO600 [8,9] and then for Advanced LIGO [10,11] and Advanced virgo [12]. This bonding technique was essential for the detectors to reach the sensitivity which enabled the detection of gravitational-wave signals from several merging binary black-hole systems [13–17] and a binary neutron-star system [18]. As the bonds have a relatively high mechanical loss, the area of the bonds must be kept small in these precision measurement applications to prevent significant thermal noise [19].

Hydroxide-catalysis bonds are also of interest for applications, in which light is transmitted through the bond, such as crystal assemblies for high-power lasers [20,21] and in optical components for precision experiments [6]. It has been shown that hydroxide-catalysis bonds between fused-silica components have low reflectivity of $< 10^{-3}$ [21,22] and a high laser-damage threshold [21], which is essential for many applications. In components like wave plates, which are composed of different materials with different properties, the damage threshold is dominated by heating due to optical absorption. While the absorption of the materials is well known and optimized for the component's design wavelength, the optical absorption of the bond layer between the materials has to be investigated.

In this paper the first measurement of the optical absorption of such bonds at several different infrared wavelengths is presented. An area of 15 mm × 15 mm, approximately in the center of the sample, was mapped in steps of 0.2 mm. While the absorption at 1064 nm was found to be too low to be easily measured accurately, the absorption at wavelengths of 1550 nm and 2000 nm was observed from one day to 38 days after bonding, showing a reduction in absorption by more than 70% on day 38 compared to the first measurement one day after bonding. The reduction in absorption appears to be the sum of two exponential decay processes, which is analyzed as a function of position on the bonded

* Corresponding author.
E-mail address: iain.martin@glasgow.ac.uk (I.W. Martin).

https://doi.org/10.1016/j.mtla.2019.100331
Received 13 January 2019; Accepted 18 April 2019
Available online 19 April 2019

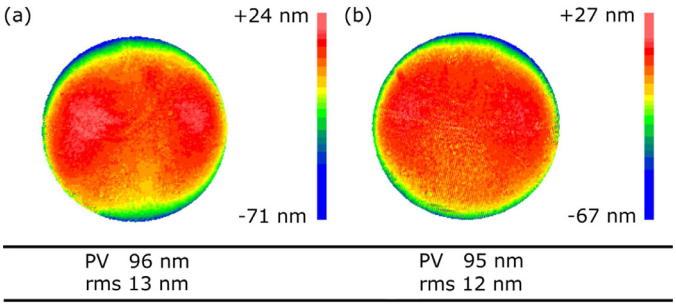

Fig. 1. Surface maps of the bonding surfaces of (a) substrate 1 and (b) substrate 2, showing the PV flatness of the substrates.

area. Analysis of the wavelength dependence of the absorption provides evidence that water migrating out of the bond may be responsible for the change in absorption observed.

2. Bonding procedure

This section gives a brief introduction to the chemistry of hydroxide-catalysis bonds and describes the procedure used to create the bonded sample studied here.

2.1. Hydroxide-catalysis bonding

The chemistry of hydroxide-catalysis bonding is described in detail in many papers [23–26]. In essence, a hydroxide solution of some form (e.g. sodium silicate or potassium hydroxide) etches into the surfaces to be bonded. This releases silicate molecules, resulting in a pH decrease of the solution. This enables the silicate molecules to form long siloxane chains, ultimately resulting in a chemical bond between the two surfaces. Water is produced as a by-product of this reaction. After the initial bond is made, the water slowly migrates out of the bond layer, either through evaporation at the edges of the bond or through migration into the substrates. Joints can be made between any silica-based materials [1,2], and other oxides (though these may benefit from added silicate molecules to the solution) [27,28]. This bonding technique is highly reliable in terms of reproducibility and strength, as long as the surfaces to be joined are extremely clean and hydrophillic at the time of bonding [20].

2.2. Sample preparation

A hydroxide-catalysis bond was made between two Corning 7979 fused silica discs, 25 mm in diameter and 6.35 mm thick. This material has low optical absorption in the infrared due to low OH content.[1] At 1064 and 1550 nm, the absorption is below the measurable level, while at 2000 nm the absorption is at a measurable level, but negligible compared to the absorption of the bond (see Section 3.3.1).

The peak-to-valley (PV) flatness of the bonding surfaces of the substrates was measured using a Zygo interferometer[2] at 633 nm. Both substrates had a convex and axisymmetric shape with an overall flatness of 95 nm (with the outer 0.25 mm trimmed off the measurement), as shown in Fig. 1. For both substrates, the central area with a diameter of 19 mm has a PV flatness of less than 30 nm. Flatness of the bonded surfaces is important to produce strong, reliable bonds with a uniform bond thickness. At the centre of the samples, where the bond absorption was measured, the bonding surfaces have a total PV flatness of $\sim$30 nm, and the rms flatness of the surfaces (equivalent to the roughness) is $\sim$12 nm. Since the bond thickness is expected to be greater than 100 nm, and possibly as high as 500 nm immediately after bonding [22], it seems unlikely that any variation in the surface roughness or flatness at this level will have a significant impact on the absorption measured in the bond.

The bonding solution was prepared by mixing one part (volumetrically) of sodium-silicate solution (Sigma Aldrich 338443) and six parts of reverse osmosis water of 18 MΩ resistance. The bonding solution was shaken, centrifuged and filtered with a 0.2 µm medical filter to ensure that no large particulates were present. Prior to bonding, the samples were cleaned using cerium-oxide paste and sodium-bicarbonate paste, and rinsed with methanol of 99.9% purity – a procedure used commonly [29,30].

Immediately before bonding, the samples were wiped with 99.9% pure methanol one more time and inspected carefully for surface defects and contaminants. 4.0 µl of bonding solution (0.8 µl/cm^2 – chosen to be the same as used for aLIGO [31]) was then deposited on one of the substrates. The other substrate was placed carefully on top. The bonded sample was left un-touched to cure for one day.

3. Optical absorption measurements

In this section the method for measuring the optical absorption of the bond is explained and the results are presented.

3.1. Measurement method

The optical absorption of the bond layer was measured using photothermal common-path interferometry [32]. In this technique, a pump beam of high power at the wavelength of interest is used to heat the sample via optical absorption. A probe beam of larger radius and lower power is used to measure the thermal effect in the sample.

Absorption of the pump beam induces a thermal lens in the material. The part of the probe beam that passes through the thermal lens interferes with the part of the probe beam that is unaffected by the thermal lens. The resulting interference pattern causes a signal proportional to the absorbed pump power. Comparison to a suitable calibration substrate of known absorption allows this signal to be converted into an absorption.

The time delay in the response of the sample to the heating contains information about the thermal diffusivity of the sample. This delay is measured as the *phase* of our absorption signal. Here, in the case of a thin bond, heat conducts rapidly into the surrounding material and the majority of the signal arises in the (comparatively thick) fused-silica regions close to the bond. The phase is therefore expected to correspond to the thermal diffusivity of fused silica. The absorption of the silica substrates is low in comparison to the bond, and any contribution of the substrate to the measured absorption of the bond is expected to be small in comparison to the error bars. The absorption of a sample can be mapped in two dimensions by moving the sample with respect to the crossing point of the pump and probe beams. The beams cross at a small angle, producing a spatial resolution in the longitudinal direction of approximately 0.5 mm. In the lateral directions, the resolution is determined by the chosen step-size, which is 0.2 mm in this case.

The absorption was measured over a period of 38 days after the samples were bonded. Most of these measurements were made at 1550 nm. However, the wavelength dependence of the absorption is of interest and some measurements at 1064 nm and 2000 nm were also carried out. A pump-beam waist of 35 µm was used, with the average laser power being $\approx$ 300 mW. For all measurements, a 1620 nm probe beam of waist 115 µm was used.

3.2. Measurement results

The optical absorption of the bond was measured over an area of the sample of 15 mm by 15 mm, in steps of 0.2 mm. A series of maps of the

[1] https://tinyurl.com/ybu4htbt.
[2] http://www.zygo.com/?/met/interferometers/gpi/.

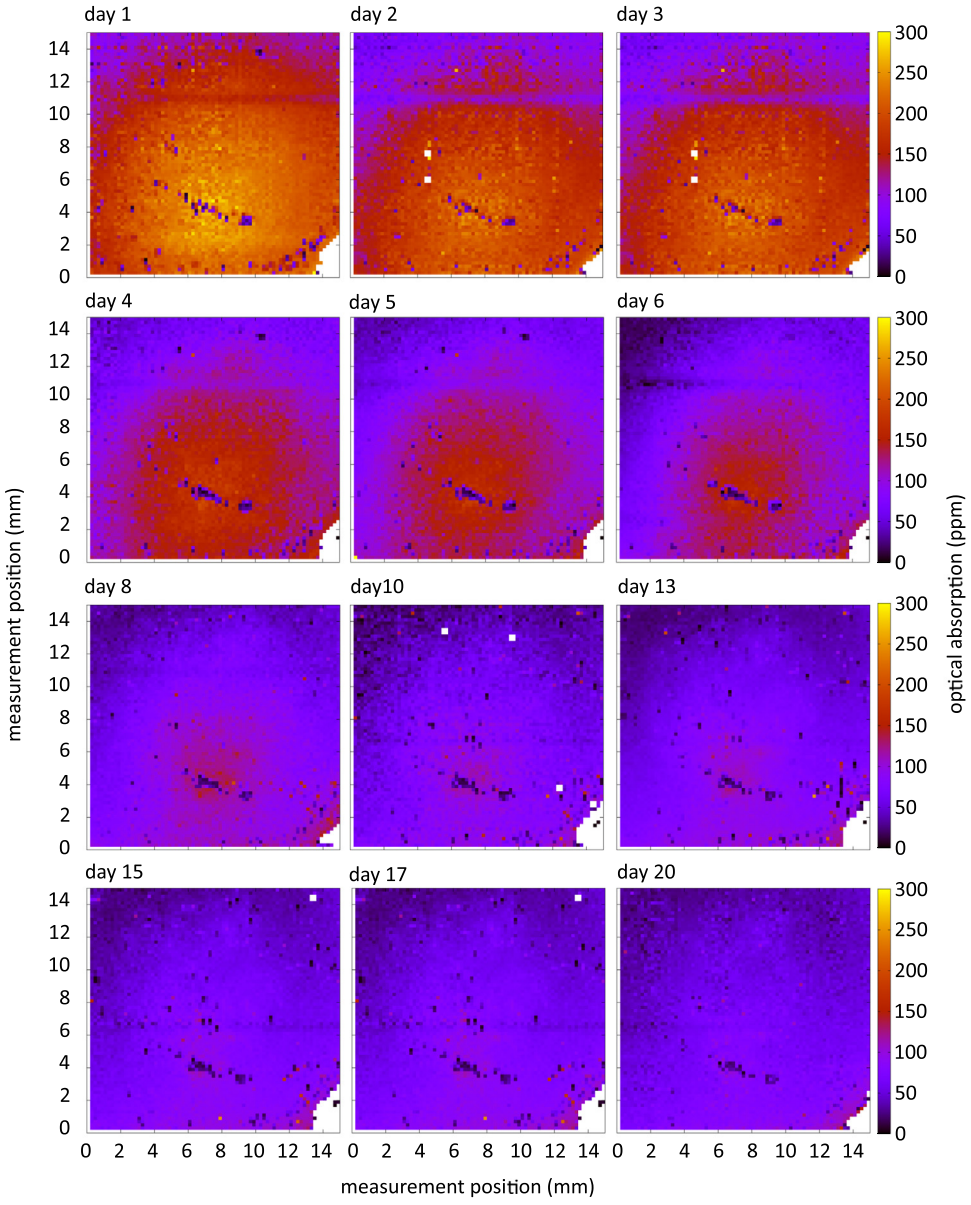

Fig. 2. Maps of the optical absorption of the bond on various days after bonding. The absorption is given in ppm (10^{-6}) per complete bond layer. (Absorption maps measured for days 23, 29 and 38 were omitted, as they appear very similar to the eye to the map for day 20.) The measured area was approximately centered in the 1" diameter sample.

absorption at 1550 nm was made over a period of 38 days after the samples were bonded, as shown in Fig. 2. Measurements were taken daily for the first 6 days as during this period the absorption was observed to decrease rapidly. Thereafter, where the absorption decreased more slowly, longer measurement intervals were used.

The absorption was found to vary significantly across the measured area of the sample, with values on the first day ranging from around 300 ppm close to the center of the measured region to around 75 ppm in one corner of the region. A linear feature was observed in many of the absorption maps (a horizontal line at a y-position of approximately 11 mm, which moves to approximately 7 mm between days 8 and 10). It is interesting to note that the feature is parallel to one of the axes on which the sample was translated, and it seems likely that it may be an artefact of the sample translation, or perhaps of sample storage orientation. However, this feature has no significant effect on the average absorption of the measured area. Some scattered points with lower absorption were also reproducibly measured close to the centre of the mapped region, which are consistent with observed air bubbles in the bond.

3.3. Measurement analysis

In this section we calculate the average absorption of the measurement region and analyse the time and spatial dependence of the measured absorption.

3.3.1. Decay of the average absorption

To obtain a comparable measure for each day, the mean absorption and standard deviation (which represents the spread of the absorption) over the entire measurement region was calculated for each map.

When calculating this average, only absorption values which had a realistic corresponding phase value between −80° and −30° were taken into account. The phase gives information about the thermal response of a particular point in the sample when it is heated. This thermal response is used in converting the measured signal into an absorption value. Points giving the 'wrong' phase have a different response and thus cannot be converted reliably into an absorption value. One possible reason for a unexpected phase values could be a poor thermal contact between the bond and the substrates [33], perhaps caused by the

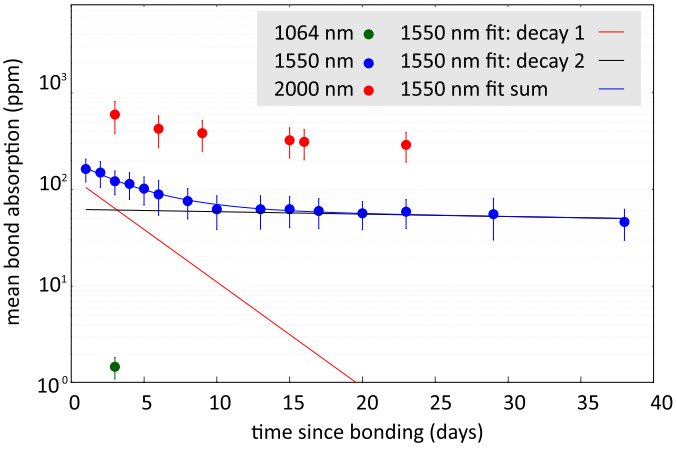

Fig. 3. Plot of the decay of the average absorption over the measurement region with time at 1550 nm and 2000 nm. For completeness, the one measurement taken at 1064 nm is included. The two exponential functions, and their sum, used to fit the 1550 nm data are also shown.

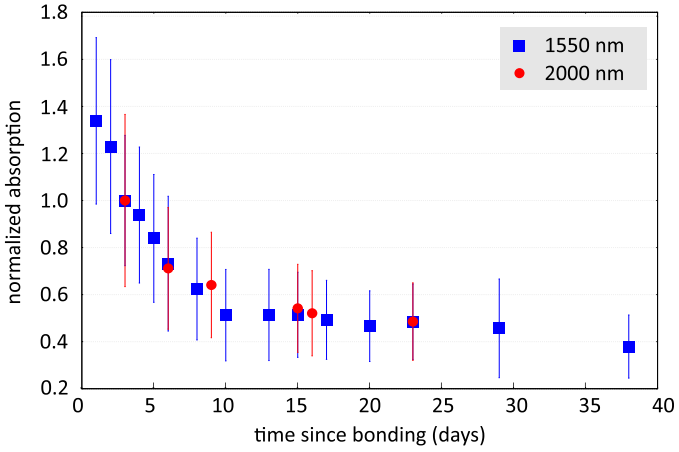

Fig. 4. Plot of the absorption against time for 1550 nm and 2000 nm, normalized to the absorption values on the 3rd day after bonding, which was the first day for which data at 2000 nm was available.

bubbles observed close to the center of the measured region, or areas of larger than average separation between the substrates.

The time evolution of the average absorption is shown in Fig. 3. The absorption decreased rapidly over the first 8 to 10 days after bonding, from an initial value of (163 ± 43) ppm at 1550 nm to (63 ± 24) ppm on day 13, and continued to decrease at a lower rate until the final measurement of (46 ± 16) ppm, 38 days after bonding. The time dependence of the absorption was fitted with a sum of two exponential decays, of the form

$$\alpha = ie^{jt} + ke^{lt}, \tag{1}$$

where α is the absorption of the bond layer, t is the time in days, and i and k are fit parameters corresponding to the initial value of the absorption for the two decays and j and l are the corresponding exponential decay constants. The fit is shown in Fig. 3 with $i = 134.9$ and $j = -2.5 \times 10^{-1}$ for the first decay and $k = 62.5$ and $l = -5.8 \times 10^{-3}$ for the second decay. Based on this equation, we can conclude back to an average absorption of 197 ppm on day 0 – directly after bonding.

While this study focused primarily on the absorption at 1550 nm, some measurements at 1064 nm and at 2000 nm were also carried out and the average absorption is shown in Fig. 3. On this scale, the background absorption of the substrates at 2000 nm was less than 8 ppm. Measurements taken at all three wavelengths on day 3 show that the absorption at 1064 nm is a factor of ∼80 lower than the absorption at 1550 nm, while the absorption at 2000 nm is a factor of ∼5 higher than the 1550 nm value. The measurement at 1064 nm was limited by noise, and it was therefore not possible to observe any further absorption decrease at this wavelength. Absorption maps at 2000 nm were measured on several other days and the relative change in absorption at 1550 nm and at 2000 nm was found to be identical throughout the measurement series, as shown in Fig. 4.

The measured change in optical absorption of hydroxide catalysis bonds is in broad agreement with past research of the evolution of other bond material properties such as reflectivity, index of refraction, bond thickness and strength [22,34]. The strength of newly formed bonds between fused silica substrates, as well as between sapphire and silicon substrates, was found to decrease slightly during the first few weeks after bonding, then stabilize at or above 15 MPa [34]. It has been suggested that the appearance of additional hydrogen bonds between the water molecules and the bond substrates during the initial bond formation leads to this trend, as the number of hydrogen bonds decreases and then disappears over time as the water migrates out of the bond. These results are correlated with other studies completed on the evolution of bond reflectivity, index of refraction, and bond thickness over similar time scales, which have indicated a initially rapid rate of change during the first weeks after bonding [22].

3.3.2. *Spatial dependence of the absorption decay*

In this section, we study the spatial dependence of the absorption in more detail. Fig. 3 suggests that there are two parts to the decay of the average absorption: a more rapid decay, which dominates the average absorption change in the first few days, and a slower decay, which fully dominates the average absorption change after day 13 (< 10 % contribution of the first decay to the total absorption). Between days 4 and 10, there are significant contributions from both of the decays. Given the large spatial variation in the absorption, it was of interest to examine the time-evolution of the absorption at every measurement point more closely.

The time-dependent absorption for every measurement point was fitted with a sum of two exponential decays – as done in Fig. 3 for the average absorption. Fig. 5 shows the results of these fits as listed below.

- (a) Shows the total absorption at day 0 (sum of fit parameters i and k).
- (b) Shows the fit parameter i, the initial absorption of the more rapid decay process.
- (c) Shows the exponential decay constant j of this decay.
- (d) Shows the total absorption (sum of i and k) for day 13.
- (e) Shows fit parameter k, the initial absorption of the slower decay.
- (f) Shows the exponential decay constant l of this decay.

Fig. 3 (c) and (f) provides a convenient way to look at the rate of change of absorption across the measured area.

Fig. 5(b) and (c) shows the fit parameters for the more rapid decay, which dominates the absorption reduction for the first few days after bonding. For this decay, the absorption can be seen to reduce more slowly in the higher-absorbing regions close to the center of the measured area, and more quickly in the lower-absorbing regions close to the edges of the measured area. A particularly rapid decay was observed in the top left of the area.

Fig. 5(e) and (f) shows the fit parameters for the slower decay, which dominates the absorption reduction from day 13 onwards. The spatial dependence of the rate of change (Fig. 5(f)) is more uniform than for the other decay (Fig. 5(c)). However, the absorption decay is slower around the edges of the area where the absorption is lower, and faster in the middle of the area where the absorption is higher.

It is interesting to note that the two decays show opposite trends, with the rapid decay particularly affecting the lower-absorbing areas

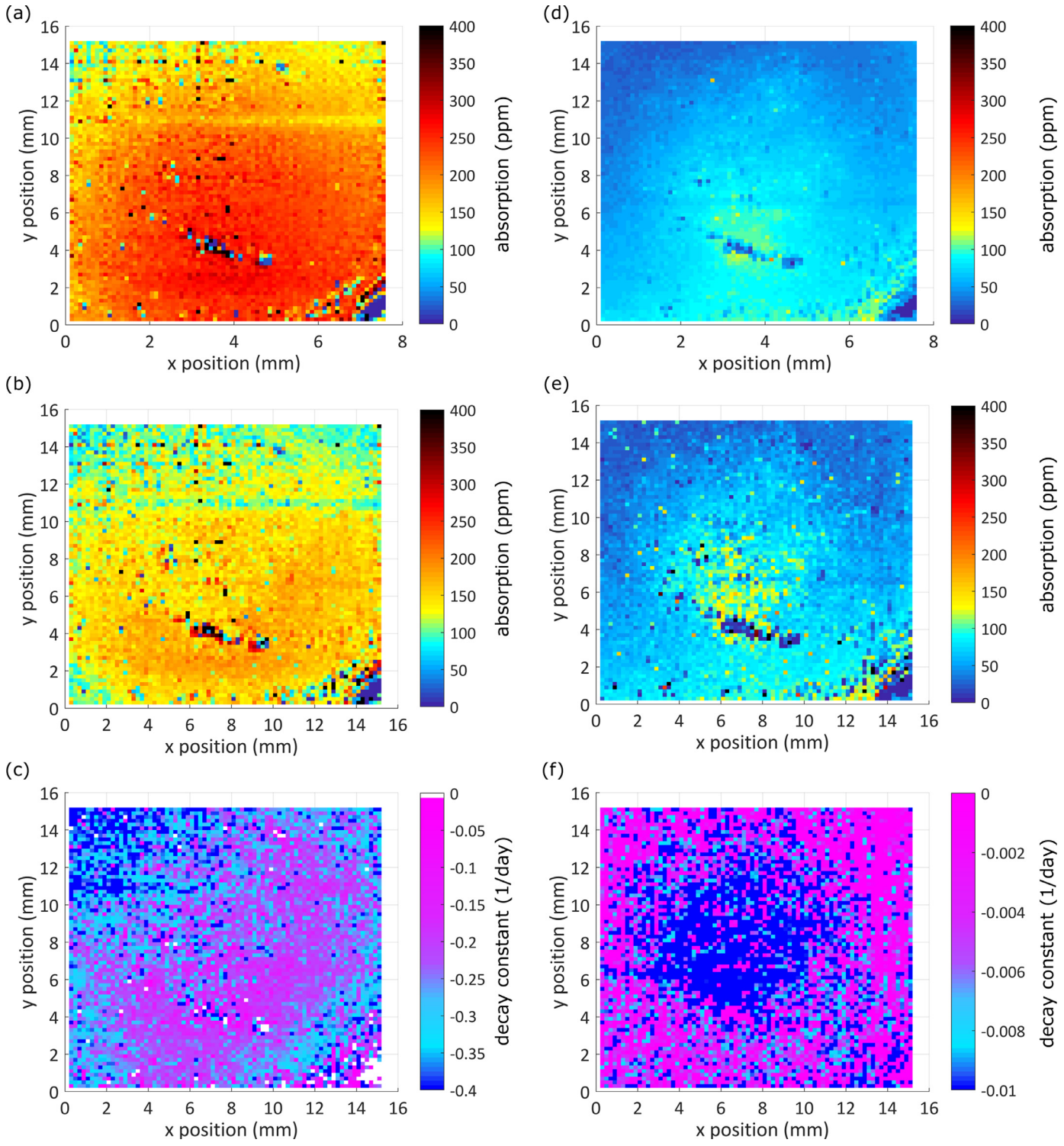

Fig. 5. Maps obtained from fitting a double-exponential decay (see Eq. 1) to the time-dependence of the absorption of every measurement point. (a) shows the total absorption (sum of fit parameters i and k) extrapolating Fig. 2 to day 0, i.e. right after bonding. (b) shows the fit parameter i, the initial absorption of the more rapid decay process (see Fig. 3) and (c) shows the exponential decay constant j of this decay. (d) shows the total absorption (sum of i and k) for day 13, at which the more rapid decay starts to be negligible (< 10 % contribution). (e) shows fit parameter k, the initial absorption of the slower decay, and (f) shows the exponential decay constant l of this decay. (Note that the two decay plots do not have the same colour key.)

near the edges and the slower decay particularly affecting the higher-absorbing region in the middle of the sample. Note that the difference in decay rate between the two decays is much larger close to the edges than in the middle.

3.4. Discussion of the absorption results

Past research has shown that the material properties of bonds such as strength, reflectivity, refractive index and thickness change over time,

stabilising as the bond cures. This is most likely due to the migration of the water initially present in the bonds [22,35].

The absorption ratio at the wavelengths investigated here is in good agreement with water absorption in the literature. The ratio of water absorption is ≈74 between 1064 nm and 1550 nm and ≈6 between 1550 nm and 2000 nm [36] compared to a factor of 82 and a factor of 5 in our bond absorption measurements. We conclude that the initial absorption is likely to be related to the water content of the bond, with the observed rapid decay being related to the water diffusing out of the bonded area.

There are two possible explanations of the slower decay shown in Fig. 3. The first is that another absorption process is present, which becomes dominant when the water content has dropped sufficiently, e.g. the absorption becomes limited by the bond material itself, which is still slowly curing with time. A different hypothesis is that both decays can be explained by water absorption. The ratio of the absorption at 1550 nm and at 2000 nm does not vary significantly over time (see Fig. 4). It seems unlikely that different absorption processes would have identical wavelength dependence, indicating that the same process is responsible for the absorption throughout the measurement series.

Fig. 5(c) shows that the lower-absorbing outer regions initially show the most rapid decay j. This is possibly related to the water migrating out of the bond faster close to the edges of the sample than in the middle. However, closer to the centre, less water migrates towards the edges, resulting in smaller values of j. At the same time, water can also migrate into the more resistant silica substrates, resulting in the underlying slower decay l (see Fig. 5(f)).

As the bond cures, it's resistance to water migration increases. Now the slower decay describing water migration into the substrate starts dominating. In the higher-absorbing centre, where the water content is high, the decay constant l is larger than in the lower-absorbing outer regions, as expected.

4. Conclusion

The time-dependence of the optical absorption of a hydroxide-catalyis bond between two fused silica samples at 1550 nm and at 2000 nm was measured. After three days, the absorption was also measured at 1064 nm. From the measurements at the different wavelengths we conclude that water is responsible for the absorption.

The absorption can be described as the sum of two exponentials decaying with time. Over the first 13 days, the absorption reduces rapidly by a factor of ≈3. As bonded optics are particularly sensitive to laser damage due to absorption, this would increase the tolerable power in a transmissive optic by the same factor. By the end of our observation period of 38 days, this factor had increased to ≈4. Assuming this trend in decay continues, then the tolerable power would increase by a factor of 6 after 100 days and by a factor of 26 after a year.

From the spatial dependence of the absorption decay, we conclude that two water-migration processes contribute to the absorption decrease: a more rapid one due to migration out of the edges of the sample and a slower one due to migration into the fused silica substrates.

Declaration of interest

None.

Acknowledgments

We are grateful for financial support from the Royal Society (RG110331), STFC (ST/N005422/1) and the University of Glasgow. Martin and van Veggel are supported by Royal Society Research Fellowships (UF150694, DH120021). We are grateful to the International Max Planck Partnership for Measurement and Observation at the Quantum Limit for support, and we thank our colleagues in the LSC and Virgo collaborations and within SUPA for their interest in this work. We would like to thank M. Phelps for many helpful comments. IWM and JS would like to thank M for getting us involved in a slightly different kind of project. This paper has LIGO Document number LIGO-P1800363.

Supplementary material

Supplementary material associated with this article can be found, in the online version, at doi:10.1016/j.mtla.2019.100331.

References

[1] D. Gwo, Ultra precision and reliable bonding method. U.S. Patent no. US 6,284,085 B1. https://patents.google.com/patent/US6284085B1/en.
[2] D. Gwo, Hydroxide-catalysed bonding, U.S. Patent no. US 6,548,176 B1. https://patents.google.com/patent/US6548176B1/en.
[3] D. Gwo, Ultra-precision bonding for cryogenic fused silica optics, in: J. Heaney, L. Burriesci (Eds.), Proceedings of the SPIE, Cryogenic Optical Systems and Instruments VIII, **3435**, 1998, p. 136.
[4] D.-H. Gwo, S. Wang, K.A. Bower, D.E. Davidson, P. Ehrenberger, et al., Hydroxide-bonding strength measurements for space-based optical missions, Adv. Space Res. 32 (2003) 1401–1405.
[5] M. Armano, H. Audley, G. Auger, Baird, et al., Sub-femto-g free fall for space-based gravitational wave observatories: Lisa pathfinder results, Phys. Rev. Lett. 116 (2016) 231101, doi:10.1103/PhysRevLett.116.231101.
[6] G. Lacaill, V. Mangano, A.A. van Veggel, C.J. Killow, P.E. MacKay, S. Rowan, J. Hough, Optical characterisation of hydroxide catalysed bonds applied to phosphate glass, Proc. SPIE 10448 (2017) pp. 10448-10448-15. doi:10.1117/12.2279693..
[7] D. Robertson, C. Killow, H. Ward, J. Hough, G. Heinzel, A. Garcia, V. Wand, U. Johann, C. Braxmaier, LTP interferometernoise sources and performance, Class. Quantum Gravity 22 (10) (2005) S155. http://stacks.iop.org/0264-9381/22/i=10/a=004.
[8] H. Grote, et al., The GEO 600 status, Class. Quantum Gravity 27 (8) (2010) 084003.
[9] B.W. Barr, G. Cagnoli, M.M. Casey, D. Clubley, et al., Silica research in Glasgow, Class. Quantum Gravity 19 (7) (2002) 1655. http://stacks.iop.org/0264-9381/19/i=7/a=357.
[10] A.V. Cumming, A.S. Bell, L. Barsotti, M.A. Barton, G. Cagnoli, D. Cook, L. Cunningham, M. Evans, G.D. Hammond, G.M. Harry, A. Heptonstall, J. Hough, R. Jones, R. Kumar, R. Mittleman, N.A. Robertson, S. Rowan, B. Shapiro, K.A. Strain, K. Tokmakov, C. Torrie, A.A. van Veggel, Design and development of the advanced LIGO monolithic fused silica suspension, Class. Quantum Gravity 29 (3) (2012) 035003. http://stacks.iop.org/0264-9381/29/i=3/a=035003.
[11] J. Aasi, et al., Advanced LIGO, Class. Quantum Gravity 32 (7) (2015) 074001. http://stacks.iop.org/0264-9381/32/i=7/a=074001.
[12] F. Acernese, et al., Advanced virgo: a second-generation interferometric gravitational wave detector, Class. Quantum Gravity 32 (2) (2015) 024001. http://stacks.iop.org/0264-9381/32/i=2/a=024001.
[13] B.P. Abbott, et al., Observation of gravitational waves from a binary black hole merger, Phys. Rev. Lett. 116 (2016) 061102, doi:10.1103/PhysRevLett.116.061102.
[14] B.P. Abbott, et al., GW151226: observation of gravitational waves from a 22-solar-mass binary black hole coalescence, Phys. Rev. Lett. 116 (2016) 241103, doi:10.1103/PhysRevLett.116.241103.
[15] B.P. Abbott, et al., GW170104: observation of a 50-solar-mass binary black hole coalescence at redshift 0.2, Phys. Rev. Lett. 118 (2017) 221101, doi:10.1103/PhysRevLett.118.221101.
[16] B.P. Abbott, et al., GW170814: a three-detector observation of gravitational waves from a binary black hole coalescence, Phys. Rev. Lett. 119 (2017) 141101, doi:10.1103/PhysRevLett.119.141101.
[17] B.P. Abbott, et al., Gw170608: observation of a 19 solar-mass binary black hole coalescence, Astrophys. J. Lett. 851 (2) (2017) L35. http://stacks.iop.org/2041-8205/851/i=2/a=L35.
[18] B.P. Abbott, et al., GW170817: observation of gravitational waves from a binary neutron star inspiral, Phys. Rev. Lett. 119 (2017) 161101, doi:10.1103/PhysRevLett.119.161101.
[19] L. Cunningham, P. Murray, A. Cumming, E. Elliffe, et al., Re-evaluation of the mechanical loss factor of hydroxide-catalysis bonds and its significance for the next generation of gravitational wave detectors, Phys. Lett. A 374 (39) (2010) 3993–3998. https://doi.org/10.1016/j.physleta.2010.07.049. http://www.sciencedirect.com/science/article/pii/S037596011000914X.
[20] A.A. van Veggel, C. Killow, Hydroxide catalysis bonding for astronomical instruments, Adv. Opt. Technol. 3 (2014) 293–307.
[21] S. Sinha, K.E. Urbanek, A. Krzywicki, R.L. Byer, Investigation of the suitability of silicate bonding for facet termination in active fiber devices, Opt. Express 15 (20) (2007) 13003–13022, doi:10.1364/OE.15.013003. http://www.opticsexpress.org/abstract.cfm?URI=oe-15-20-13003.
[22] V. Mangano, A.A. van Veggel, R. Douglas, J. Faller, A. Grant, J. Hough, S. Rowan, Determination of the refractive index and thickness of a hydroxide-catalysis bond between fused silica from reflectivity measurements, Opt. Express 25 (4) (2017) 3196–3213, doi:10.1364/OE.25.003196. http://www.opticsexpress.org/abstract.cfm?URI=oe-25-4-3196.
[23] E.J. Elliffe, J. Bogenstahl, A. Deshpande, J. Hough, et al., Hydroxide-catalysis bonding for stable optical systems for space, Class. Quantum Gravity 22 (10) (2005) S257–S267, doi:10.1088/0264-9381/22/10/018. http://stacks.iop.org/0264-9381/22/S257.

[24] H.S. Kim, T.L. Schmitz, Shear strength evaluation of hydroxide catalysis bonds for glass-glass and glass-aluminum assemblies, Precis. Eng. 37 (1) (2013) 23–32, doi:10.1016/j.precisioneng.2012.06.004. http://www.sciencedirect.com/science/article/pii/S0141635912000980.

[25] A.A. van Veggel, J. Scott, D.A. Skinner, B. Bezensek, W. Cunningham, J. Hough, I. Martin, P. Murray, S. Reid, S. Rowan, Strength testing and sem imaging of hydroxide-catalysis bonds between silicon, Class. Quantum Gravity 26 (17) (2009) 175007. http://stacks.iop.org/0264-9381/26/i=17/a=175007.

[26] N.L. Beveridge, A.A. van Veggel, M. Hendry, P. Murray, R.A. Montgomery, E. Jesse, J. Scott, R.B. Bezensek, L. Cunningham, J. Hough, R. Nawrodt, S. Reid, S. Rowan, Low-temperature strength tests and sem imaging of hydroxide catalysis bonds in silicon, Class. Quantum Gravity 28 (8) (2011) 085014. http://stacks.iop.org/0264-9381/28/i=8/a=085014.

[27] R. Douglas, A.A. van Veggel, L. Cunningham, K. Haughian, J. Hough, S. Rowan, Cryogenic and room temperature strength of sapphire jointed by hydroxide-catalysis bonding, Class. Quantum Gravity 31 (4) (2014) 045001.

[28] E.J. Elliffe, J. Bogenstahl, A. Deshpande, J. Hough, C. Killow, S. Reid, D. Robertson, S. Rowan, H. Ward, G. Cagnoli, Hydroxide-catalysis bonding for stable optical systems for space, Class. Quantum Gravity 22 (10) (2005) S257. http://stacks.iop.org/0264-9381/22/i=10/a=018.

[29] A. van Veggel, D. van den Ende, J. Bogenstahl, S. Rowan, W. Cunningham, G. Gubbels, H. Nijmeijer, Hydroxide catalysis bonding of silicon carbide, J. Eur. Ceram. Soc. 28 (1) (2008) 303–310, doi:10.1016/j.jeurceramsoc.2007.06.002. http://www.sciencedirect.com/science/article/pii/S0955221907003809.

[30] A. Preston, B. Balaban, G. Mueller, Hydroxide-bonding strength measurements for space-based optical missions, Int. J. Appl. Ceram. Technol. 5 (4) (2008) 365–372.

[31] A.A. van Veggel, Silicate bonding procedure, LIGO technical document E050228 https://dcc.ligo.org/LIGO-E050228-v2/public.

[32] A.L. Alexandrovski, M.M. Fejer, A. Markosyan, R. Route, Photothermal common-path interferometry (PCI): new developments, in: Proceedings of the SPIE 7193, Solid State Lasers XVIII: Technology and Devices, 71930D, 2009, doi:10.1117/12.814813.

[33] J. Steinlechner, I.W. Martin, A. Bell, G. Cole, J. Hough, S. Penn, S. Rowan, S. Steinlechner, Mapping the optical absorption of a substrate-transferred crystalline algaas coating at 1.5μm, Class. Quantum Gravity 32 (10) (2015) 105008. http://stacks.iop.org/0264-9381/32/i=10/a=105008.

[34] M. Phelps, M.M. Reid, R. Douglas, A.-M. van Veggel, V. Mangano, K. Haughian, A. Jongschaap, M. Kelly, J. Hough, S. Rowan, Strength of hydroxide catalysis bonds between sapphire, silicon, and fused silica as a function of time, Phys. Rev. D 98 (2018) 122003, doi:10.1103/PhysRevD.98.122003.

[35] R.K. Iler, The Chemistry of Silica, John WIley and Sons, 1979.

[36] K.F. Palmer, D. Williams, Optical properties of water in the near infrared, J. Opt. Soc. Am. 64 (1974) 1107–1110. https://www.osapublishing.org/josa/abstract.cfm?uri=josa-64-8-1107.